This is an *Accepted Manuscript*, which has been through the Royal Society of Chemistry peer review process and has been accepted for publication.

Accepted Manuscripts are published online shortly after acceptance, before technical editing, formatting and proof reading. Using this free service, authors can make their results available to the community, in citable form, before we publish the edited article. We will replace this *Accepted Manuscript* with the edited and formatted *Advance Article* as soon as it is available.

You can find more information about *Accepted Manuscripts* in the **Information for Authors**.

Please note that technical editing may introduce minor changes to the text and/or graphics, which may alter content. The journal's standard **Terms & Conditions** and the **Ethical guidelines** still apply. In no event shall the Royal Society of Chemistry be held responsible for any errors or omissions in this *Accepted Manuscript* or any consequences arising from the use of any information it contains.

ARTICLE

Polymer Chemistry Accepted Manuscript

Modular amphiphilic copolymer-grafted nanoparticles: "nanoparticle micelle" behavior enhances utility as dispersants

Muhammad Ejaz,[a] Alina M. Alb,[b] Karolina A. Kosakowska,[a] and Scott M. Grayson[a],*

The majority of existing dispersant systems are based on small molecule amphiphiles and therefore are susceptible to disaggregation when sufficiently diluted. An alternative design is proposed using nanoparticles as a core to template amphiphilic polymers grafted onto their surface into a micelle-like conformation. Such amphiphilic "nanoparticle micelles" will not disaggregate upon dilution, similar to unimolecular micelles. These nanodispersants were prepared by grafting successive blocks of poly(ε-caprolactone) and poly(ethylene glycol) from functionalized silica nanoparticles through a combination of surface-initiated ring-opening polymerization and activated ester conjugation chemistry. The swellable hydrophobic poly(ε-caprolactone) inner block enabled the encapsulation of a hydrocarbon payload while the hydrophilic poly(ethylene glycol) outer block afforded stable dispersions in aqueous media. Their capacity for hydrocarbon encapsulation was confirmed by their ability to sequester ultraviolet active dyes in aqueous environments and because the length of the polymer blocks can be easily tuned, this design enables the optimization of their loading capacity. Additional characterization using light scattering-based methodologies combined with ultraviolet spectroscopy, ^{1}H nuclear magnetic resonance, Fourier transform infrared spectroscopy, transmission electron microscopy, and thermogravimetric analysis experiments confirmed the nanodispersant structure and their "unimolecular micelle-like" behavior.

Introduction

Traditional dispersants are small amphiphilic molecules that encourage the formation of oil microdroplets (~ 50 μm in diameter) by assembling at their interface with bulk water. Although such dispersant-stabilized emulsions may exhibit short-term stability, dilution in large volumes of water causes the continuous depletion of surfactant molecules from the microdroplet interface via their transfer into bulk water which ultimately destabilizes these assemblies.[1,2] This destabilization can be thought of as analogous to the intrinsic instability micelles composed of small molecule amphipihiles in an open system. When such micelles are diluted, the reversible association/disassociation of the interface-stabilizing surfactants into the aqueous phase eventually causes the micelles to fall apart, and the concentration at which disaggregation is favored has been referred to as the critical micelle concentration (cmc). One attractive way to combat this instability to dilution involves compositions in which the individually amphiphilic units are covalently tethered together to prevent their disaggregation. Such structures have been termed "unimolecular micelles"[3] and have been prepared from dendrimers,[4-6] hyperbranched polymers,[7,8] star polymers,[9,10] and graft polymers.[11,12] While the

concept of unimolecular micelles has been explored extensively for drug delivery applications, few studies have addressed their potential application as dispersants.

One noteable example of dispersants based on amphiphilic nanostructures utilized the attachment of amphiphilic block copolymers to iron nanoparticle cores, which also provides an elegant means of recapture via application of an external magnetic field.[13] However, the study described below focuses instead on amphiphilic nanostructures that are comprised of polymers and nanoparticles that are both relatively biocompatible, so as to avoid the need for recapture. Because a competitive dispersant technology must be highly cost-efficient as well as environmentally benign, only a limited number of components met these criteria. Silica nanoparticles (SiO$_2$NPs) were selected as a core because of silica's biocompatible, as well as their synthetic optimization and commercial availability of SiO$_2$NPs in a range of sizes.[14] While the surface functionalization of SiO$_2$NPs is well established, only a few examples with amphiphilic block copolymers have been investigated to date.[15-18]

The polymer grafts can be introduced onto the nanoparticle surface using either a *"graft to"* approach with preformed polymers[19] or a *"graft from"* approach via surface initiated polymerization[20]; however, only the latter provides polymer brushes of the sufficient thickness to significantly alter the physical properties of the nanoparticles.[21] In order to pursue this route, the surface first had to be modified with a silanizing reagent to introduce stable functional groups for the *"graft-from"* polymerization. Next, poly(ε-caprolactone) (PCL) was targeted as the hydrophobic polyester inner block, via the ring opening polymerization[22] of ε-caprolactone (CL)[23-26] because it is both

a. *Tulane University, Chemistry Department, New Orleans, LA, USA.*
E-mail: sgrayson@tulane.edu
b. *Tulane University, Physics and Engineering Physics Department, New Orleans, LA, USA.*
†Electronic Supplementary Information (ESI) available: Experimental part and additional figures. See DOI: 10.1039/x0xx00000x

biocompatible and biodegradable. Finally, poly(ethylene glycol) (PEG) was selected as the hydrophilic outer block due to its water solubility and biocompatibility, and could be attached to the terminal hydroxy group of the PCL grafts via activated ester coupling.

Upon successful nanoparticle surface activation, CL polymerization, and PEG coupling, the resulting amphiphilic nanoparticles exhibited stable dispersion in aqueous media, confirming the presence of dense amphiphilic grafts. Based on their design, the proposed nanoparticle micelles are expected to exhibit long term stability even under highly dilute conditions, unlike traditional small-molecule dispersants. This significant advantage of the amphiphilic nanoparticles was confirmed by subjecting them to comprehensive characterization using a combination of techniques based on light scattering (LS) and ultraviolet spectroscopy (UV). In addition, the inherent modularity of the synthetic route enabled the encapsulation capacity to be tuned by controlling the length of the hydrophobic PCL block.

Results and discussion

Synthesis and characterization of the amphiphilic SiO$_2$NP-PCL-PEG copolymer grafted nanoparticles

The synthesis of silica core/amphiphilic copolymer shell nanoparticles was achieved using a three step process: 1) the grafting of hydroxyl groups onto the surface to provide appropriate functional groups from which to initiate polymerization, 2) the surface-initiated ring opening polymerization (SIROP) of ε-caprolactone to generate the hydrophobic inner block and 3) the conjugation of carboxy-functionalized PEG using activated ester coupling to afford the hydrophilic outer block (Scheme 1). This synthetic design was targeted due to the wide availability of each of the starting materials and the technical simplicity of the reaction sequence.
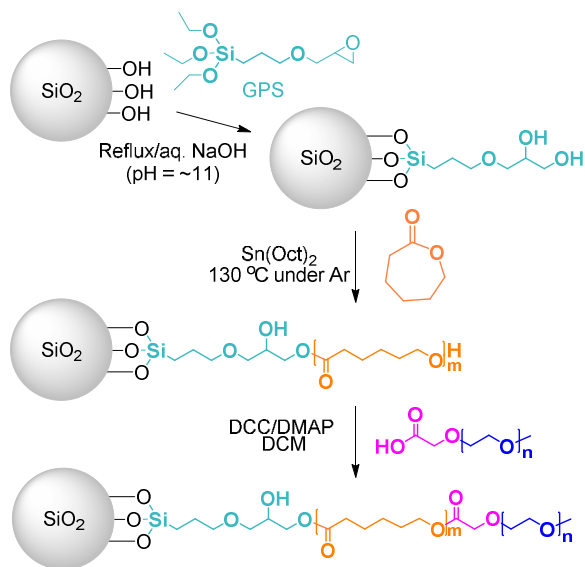
Scheme 1 Synthesis of amphiphilic polymer grafts from SiO$_2$NP cores utilizing SIROP of CL, followed by activated ester coupling with a PEG carboxylic acid.

Silica nanoparticles: initial characterization and surface modification. Before pursuing their surface modification, the commercially available SiO$_2$NPs were characterized to confirm their

well-defined structure. TEM images of the nanoparticles in Fig. 1a show unagglomerated particles with an average diameter of 70-100 nm. Dynamic light scattering (DLS) measurements for the diluted SiO$_2$NPs in isopropanol determined an average intensity-average hydrodynamic diameter (D_h) value of ~ 135 nm and narrow polydispersity (PDI) ~ 0.1, confirming that they are readily dispersed under these solvent conditions (Fig. S1).
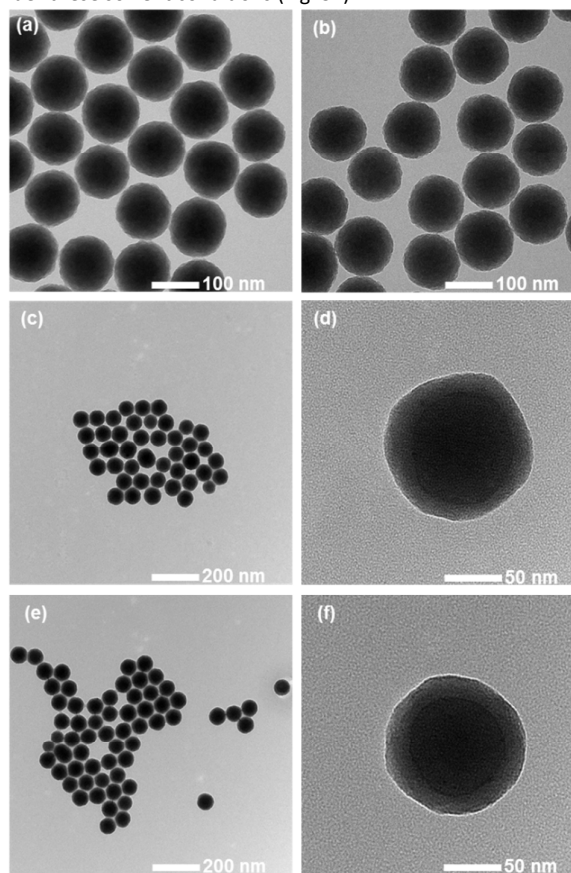
Fig. 1 TEM images of (a) as-received SiO$_2$NPs and (b) SiO$_2$NP-GPS confirm they are discrete particles with narrow dispersity, TEM images of (c) SiO$_2$NP-PCL and (d) SiO$_2$NP-PCL (high resolution) verify an increase in size upon grafting and TEM images of (e) SiO$_2$NP-PCL-PEG and (f) SiO$_2$NP-PCL-PEG (high resolution) confirm the presence of a polymer corona on the nanoparticles.

The FTIR of the same SiO$_2$NPs shown in Fig. 2a confirmed a predominantly silica composition with the asymmetric Si-O-Si stretch (1000-1250 cm^{-1}) and the asymmetric stretching vibration of Si-OH (800 cm^{-1}).
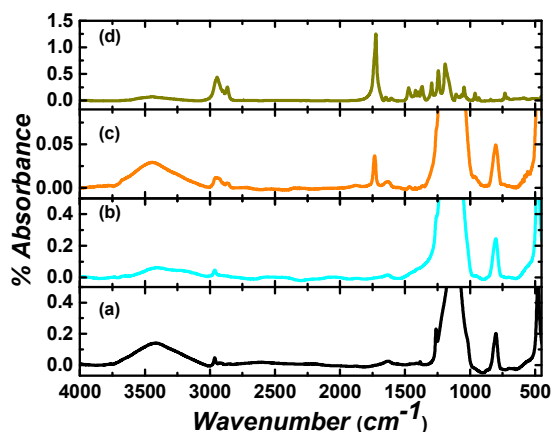
ARTICLE

Fig. 2 FTIR spectra of (a) SiO$_2$NPs, (b) SiO$_2$NP-GPS, (c) SiO$_2$NP-PCL, and (d) pure PCL verify the grafting of PCL onto the nanoparticles using SIROP.

Thermogravimetric analysis (TGA) data (Fig. 3a) verified that the SiO$_2$NPs are stable up to 800 °C without significant mass loss, with only 2.7 % mass loss observed below 600 °C, attributed to trace surface absorbed materials.

Before polymer could be grafted onto these well-defined SiO$_2$NPs, a surface functionalization was required to anchor appropriate polymer initiator groups for SIROP polymerization, as a stable linkage to the polyester chains cannot be generated by directly grafting from the native silanol surface. This functionalization was achieved using the one-step chemical condensation reaction of 3-glycidoxypropyl)triethoxysilane (GPS) with the silanol surface of the SiO$_2$NPs. The basic aqueous reaction conditions also led to a simultaneous hydrolysis of the epoxy group to yield the desired alcohol initiating groups.[27]

FTIR analysis of the SiO$_2$NP-GPS product (Fig. 2b) indicates a negligible change in the absorption spectra upon reaction with GPS, as expected because the weight percentage of surface GPS groups is small relative to the bulk silica core. The TEM image of the diol-functionalized SiO$_2$NPs in Fig. 1b also appears largely unchanged, but confirm that these particles are not aggregated or chemically cross-linked during the functionalization step. TGA data for the SiO$_2$NP-GPS exhibited only a small mass loss, about 3.9 %, below 600 °C (Fig. 3b). Therefore, the difference in mass loss at 600 °C for the SiO$_2$NP-GPS relative to that of the unmodified starting material (2.7%) was about 1.2 %, consistent with the proposed surface functionalization which should exhibit a negligible mass change relative to the bulk SiO$_2$NPs.
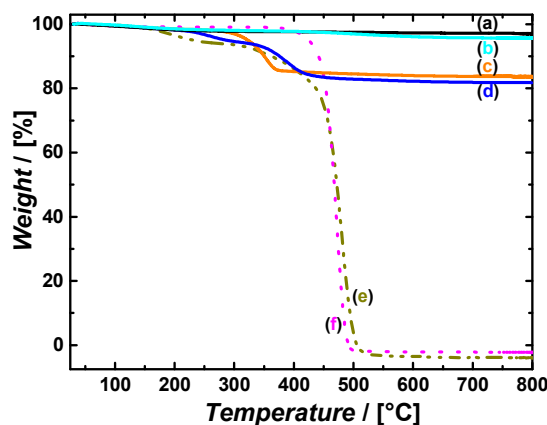

Fig. 3 TGA data for (a) SiO$_2$NP, (b) SiO$_2$NP-GPS, (c) SiO$_2$NP-PCL, (d) SiO$_2$NP-PCL-PEG, (e) pure PCL, and (f) pure PEG confirm the addition of mass to the nanoparticles after each grafting step.

PCL grafted nanoparticles: synthesis and characterization. With a hydroxyl-functionalized surface, these particles were now amenable to grafting polyesters. The SIROP of CL was performed in bulk in a two-neck round bottom flask under Ar at 130 °C using Sn(Oct)$_2$ as the catalyst. It is believed that PCL grafting occurs predominantly from the primary hydroxyl groups as the secondary hydroxyl groups are more sterically hindered, inhibiting initiation from those sites.[25] Although no free (unattached) initiator is added, free polymer is formed, presumably from adventitious water. Because the free polymer was formed under identical polymerization conditions as the grafted polymer, it was used to crudely approximate the molecular weight of the polymer grafts.

In order to isolate the grafted nanoparticles (SiO$_2$NP-PCL) from free polymers, the product was dissolved in THF, centrifuged, the supernatant removed, and the particles resuspended in solvent. This sequence was repeated 5 times to assure the removal of any polymer that was not covalently attached to the nanoparticles. The FTIR spectrum of SiO$_2$NP-PCL in Fig. 2c indicates a significant new absorption at 1734 cm^{-1}, attributed to the C=O stretching of the ester (observed at 1734 cm^{-1} for free PCL) and a weaker absorption at 2935 cm^{-1}, consistent with the C-H stretching (observed at 2914 cm^{-1} for free PCL) providing strong evidence for the presence of PCL grafts. The other characteristic absorption band for PCL, the C-O stretch at 1245 cm^{-1} overlapped with the region of the Si-O-Si asymmetric stretching vibration band (1000 and 1250 cm^{-1}) preventing its visualization.

Next, in order to characterize the PCL grafts on the nanoparticles, the chains were cleaved from the surface using an aqueous HF treatment of the polymer-silica hybrid particles[28,29] and

compared to the free PCL generated as a byproduct. Weight average molecular weight (M_w) values of 7400 g mole^{-1} and 12,000 g mole^{-1} and narrow dispersity (~ 1.1) values for the free and cleaved PCL, respectively, were obtained by Size Exclusion Chromatography (SEC) with THF as solvent and PCL standards as calibrants (Fig. S2). To confirm the relative accuracy of the molecular weight determination by SEC, MALDI molecular weight data for the free PCL was also acquired (Fig. S3).

A typical TEM image of PCL grafted silica nanoparticles is shown in Fig. 1c. The PCL layer can be seen as a translucent corona, relative to the more opaque silica cores that inhibit electron transmission. The grafted nanoparticles were well-resolved and did not exhibit any inter-particle aggregation. Based on the increased nanoparticle radii observed in the TEM images, the average thickness of the PCL grafted films was estimated to be ~ 15 nm. The presence of a thick PCL layer was confirmed during thermal analysis (Fig. 3c) which exhibited a significant change in the total mass loss (~ 16.0 %) at 600 °C which corresponds to 12.1% of the mass attributed to PCL. The bulk of the observed loss occurred between 300 and 500 °C, a similar temperature to the thermal decomposition of free PCL (Fig. 3e).

The grafting density, Σ, of the PCL layer could be approximated from the equation:[30]

$$\Sigma = \Gamma x 10^{-21} N_A / M_n \qquad (1)$$

where N_A is Avogadro's number and M_n is the absolute number average molecular weight.

The surface coverage, Γ, was calculated as the ratio of the weight fraction of the grafted PCL to that of the nanoparticle (0.121 g/g), obtained from TGA data and the specific surface area of the bare silica substrate (20 m^2 g^{-1}), determined from the relationship between the particle size of non-porous spherical silica and specific surface area.[31] The computed Γ = 6.05 mg m^{-2} value allowed the grafting density, Σ, of the PCL layer to be computed from eq. (1) as 0.304 chains/nm^2, using M_{PCL} = 12,000 g mole^{-1} based on the SEC of the cleaved PCL. This was similar to the graft densities previously reported for PCL on silica (~0.4-0.7 chains/nm^2).[27]

Further confirmation of successful polymer grafting is seen in Fig. 4 in the evolution of the radius of gyration, R_g, computed from multi-angle LS data collected continuously during a SIROP of CL. The observed increase in R_g with respect to reaction time is primarily attributed to the growth of PCL chains grafted onto the SiO$_2$NPs, as the short free PCL chains also produced during reaction (R_g ~ 4 nm), have a negligible contribution to the average size of the mixture of PCL-grafted nanoparticles and free PCL.

Synthesis of the amphiphilic SiO$_2$NP-PCL-PEG nanoparticles. In order to provide the hydrophilic corona for the grafted nanoparticles, hydrophilic HOOC-PEG-OCH$_3$ was grafted to the hydroxy end groups of the grafted PCL chains. PEG was selected as the hydrophilic block because its non-ionic character minimizes pH dependence, while avoiding the cytotoxicity associated with hydrophilic polycations. The coupling reaction was achieved using DCC with a DMAP catalyst to generate the activated ester. The retention of the strong carbonyl bands in the FTIR spectrum of SiO$_2$NP-PCL-PEG in Fig. 5b, at 1734 cm^{-1}, confirms that the bulk of the PCL grafts were retained during this ester coupling step.
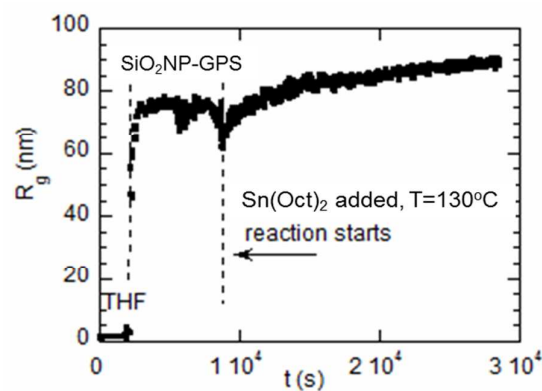

Fig. 4 R_g evolution during an online monitored SIROP of CL measures the steady growth in nanoparticle size during the PCL grafting reaction.

A number of subtle changes in the IR spectra were observed that are consistent with the attachment of PEG grafts, including an enhanced intensity of absorption between 2800 and 3000 cm^{-1} due to the C-H stretching and the appearance of a slight shoulder at about 1361 cm^{-1} which is attributed to the CH$_2$O- groups of the PEG grafts. However, the most convincing evidence for the attachment of the PEG block is the significant ease with which the PEG-grafted nanoparticles could be suspended in water, in contrast to their SiO$_2$NP-PCL precursors.
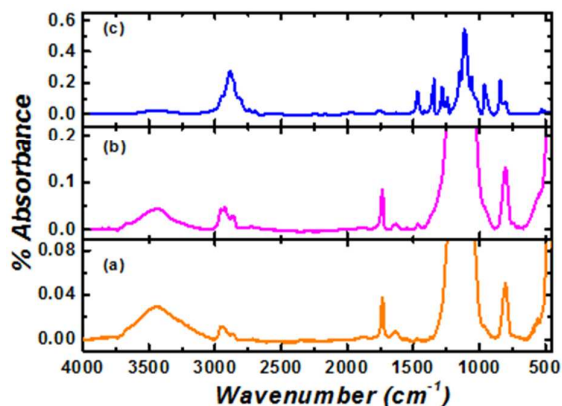

Fig. 5 FTIR spectra of (a) SiO$_2$NP -PCL, (b) SiO$_2$NP -PCL-PEG, and (c) pure PEG are consistent with the attachment of PEG.

The unaggregated nature of SiO$_2$NP-PCL-PEG was again confirmed by the TEM (Fig. 1e), where these nanoparticles exhibit a closely packed two-dimensional array rather than a three-dimensional agglomeration that might suggest physical cross-linking.

The TGA data for the SiO$_2$NP-PCL-PEG showed a 17.8 % total weight loss (Fig. 3d), only a slight increase (1.8 %) over the 16.0 % observed before the PEG conjugation reaction (Fig. 3c). While the significantly improved ability to suspend the SiO$_2$NP-PCL-PEG in water confirms their surface modification with PEG, the relatively small change in TGA weight loss can be attributed to the relatively low molecular weight of the PEG block (between one half and one third that of the PCL block) in addition to non-quantitative PEGylation of the PCL grafts. In order to quantify the ratio of PEG to PCL, the SiO$_2$NP-PCL-PEG were treated with HF to isolate free block copolymer, and the block ratio determined by ^{1}H NMR (Fig. S4-S10). ^{1}H NMR integration determined a PEG to PCL ratio of 1.0 to 4.0 repeat units, respectively. Given a PEG molecular weight of 3360

(calculated by MALDI-TOF MS) and a PCL molecular weight of 12,000 (calculated by SEC), this suggests that 34.8 % of PCL chain ends have been functionalized with a PEG block. For the observed 17.8 % weight loss observed by TGA, this block ratio would correspond to 12.7 % of the weight loss resulting from the PCL block alone. This value is in close agreement with the observed value of 12.1 % weight loss for the PCL block alone. As an additional confirmation of the attachment of PEG, the PEG-PCL functionalized nanoparticles could be reacted with sodium hydroxide to complete degrade the PCL, enabling the PEG (and degraded PCL) to be characterized by NMR and MALDI-TOF MS (Fig. S11-S13). These data also suggest approximately one third of the PCL grafts were PEGylated. Although the PEGylation coupling reaction was not quantitative, the amphiphilic SiO$_2$NPs exhibited the desired stability in aqueous suspensions, as well as unique encapsulation capabilities of hydrophobic guests, which are described in detail below.

Studies on the stability of the SiO$_2$NP-PCL-PEG copolymer grafted nanoparticles and their effectiveness in encapsulating small hydrophobic molecules

Because hydrophobic core/hydrophilic shell architectures have the potential to sequester hydrophobic molecules in aqueous environments, experiments were designed to determine the major factors that influence the encapsulation performance of these amphiphilic nanoparticles, including their dispersibility in aqueous media, their particle size and stability, and their loading capabilities. Because of the modularity of the synthetic protocol, parameters such as the length of the polymer blocks can be easily tuned in order to optimize the design for specific applications.

Nanoparticles stability in aqueous environment. DLS experiments were used to examine aqueous solutions containing nanoparticles at each stage of their surface modification: the bare SiO$_2$NP; the surface-functionalized SiO$_2$NP-GPS; the hydrophobic, grafted SiO$_2$NP-PCL; and finally, the amphiphilic copolymer-grafted SiO$_2$NP-PCL-PEG. The data confirmed that the nanoparticles were rather stable when dispersed in aqueous media (for weeks to months) and exhibited homogeneous particle distributions, with the notable exception of the hydrophobic PCL grafted nanoparticles which exhibited poor stability and a tendency to aggregate in aqueous media (Fig. S14), though they could be readily dispersed in organic solvents such as tetrahydrofuran, dichloromethane, or toluene.

Listed in Table 1 are D_h values averaged over multiple DLS measurements for each of the aqueous nanoparticle solutions. The particle sizes increase as expected with each modification of the SiO$_2$NP surface. While the distributions for the other three nanoparticles are narrow and reproducible, the D_h value is not

reported for the PCL grafted nanoparticles because their hydrophobic nature causes unstable aggregates of irreproducible size, as is expected for poorly solvated nanoparticles (Fig. S14).

Table 1 Intensity-averaged D_h values from multiple DLS measurements made on aqueous solutions containing the SiO$_2$NPs at different stages of their surface functionalization.

	SiO$_2$NP	SiO$_2$NP-GPS	SiO$_2$NP-PCL	SiO$_2$NP-PCL-PEG
D_h (nm)	150±3	156±4	NA^a	211±4

^{a} highly aggregated particle clusters, due to solution poor quality given their hydrophobic nature

Because these nanoparticle dispersants might be applied to a wide range of aqueous conditions (fresh water, salt water, etc.) and temperatures, the behavior of the SiO$_2$NP-PCL-PEG was explored in deionized water, a solution of 0.6 M NaCl and water taken from the Gulf of Mexico as well as a range of temperatures. As expected, based upon their covalent design, the nanoparticles exhibited minimal variations in size with changes in aqueous media or in temperature (Table S3, Fig. S15).

Initial guest-host encapsulation LS and UV studies. The critical parameter for defining the utility of the amphiphilic nanoparticles is their encapsulation capacity and its stability with time. The effectiveness of the SiO$_2$NP-PCL-PEG copolymer grafted nanoparticles to encapsulate small hydrophobic molecules was first investigated by LS measurements. 4-Heptylphenol (Hph) was chosen as a model compound for small molecule sequestration, due to its high solubility in non-polar organic media, limited solubility in aqueous media, strong UV absorbance, and biological relevance.[32]

Light scattering profiles of aqueous mixtures of grafted nanoparticles and Hph were compared, during DLS experiments, to the scattering of each individual component in order to elucidate their possible interaction and assess the loading capabilities of the amphiphilic copolymer-grafted nanoparticles. It is well-known for non-interacting bicomponent mixtures that scattering signal is additive and given by the sum of individual contributions from each component; however, for interactive systems, a non-additive scattering profile of the mixture is observed.

For a multicomponent system, the general expression for the excess scattering (i.e. total scattering minus solvent scattering background) for a system of N components is:

$$I(q) \propto \sum_{i,j=1}^{N} a_i S_{ij}(q) a_j \qquad (2)$$

where q is the scattering vector, $q = (4\pi n/\lambda)\sin(\theta/2)$, n is the index of refraction of the solvent, λ is the vacuum wavelength of the laser, θ is the scattering angle, $a_{i(j)}$ is the differential refractive index for species i(j), $a_{i(j)} = (\partial n/\partial c)_{i(j)}$, c_i is the concentration of species i(j), and the S_{ij} terms are the partial structure factors.[33] If the interactions between two different species are repulsive, then $S_{ij} < 0$ and the total scattering of the mixture will be less than the sum of the total scattering of the individual species. Similarly, for attractive interactions between the system components, the total scattering will be greater than the sum of the individual scattering, whereas for zero or negligible interactions, the total scattering should be just the sum of the individual species' scattering.

Shown in Fig. 6 are data from DLS experiments made on SiO$_2$NP-PCL-PEG and SiO$_2$NP-GPS nanoparticles dispersed in water (0.00625 mg mL^{-1}), in which Hph was added (0.033 mg mL^{-1}); data from individual components of the respective systems are also shown. In the absence of any interaction between Hph and the functionalized nanoparticles, the total scattering of their mixtures should be additive, and in this case, since Hph small molecules

multi-size distribution (MSD) data (Fig. S16) were seen (within the conditions studied) at the addition of Hph. This confirms that the observed interactions are not caused by association/aggregation between nanoparticles, but rather encapsulation of the Hph by the amphiphilic nanoparticles.

Stability to dilution: "nanoparticle micelle" behavior of the copolymer grafted nanoparticles. One of the main drawbacks of carrier systems based on micelles of linear amphiphilic block copolymer or small molecule amphiphiles is their instability upon dilution.[35-37] Thus, at concentrations below cmc, micelles tend to disassemble causing changes in both structure and size that compromise their controlled encapsulation of small guest molecules. In contrast, the unique design of grafted nanoparticles comprised of a hydrophobic inner shell and a hydrophilic outer shell confers "micelle-like" properties onto the amphiphilic silica particles, each individual nanoparticle behaving as an individual micelle.[3,38-40] Their micellar structure is reinforced by covalently linkages to the nanoparticle core and, therefore, these micelles should not disaggregate when diluted. As a result, they should
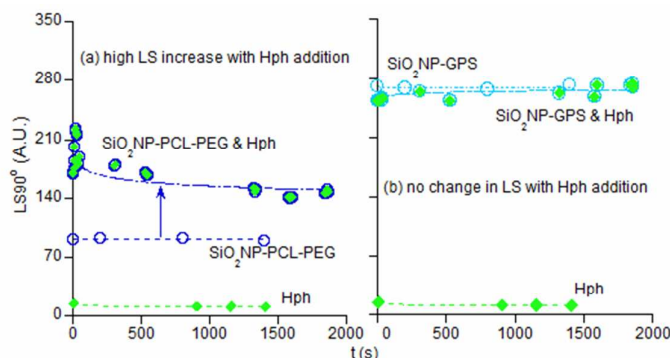

Fig. 6 LS90^o data for (a) SiO$_2$NP-PCL-PEG&Hph and (b) SiO$_2$NP-GPS&Hph aqueous mixtures compared to scattering of the individual components, respectively, illustrate the interactive behavior with the grafted amphiphilic nanoparticles with Hph *vs*. non-interactive behavior with the ungrafted nanoparticles.

alone do not scatter significantly, total scattering should be only slightly higher than observed for the functionalized nanoparticles alone. Such behavior is observed during the addition of Hph to the SiO$_2$NP-GPS (Fig. 6b), confirming that there is no interaction observed between the nanoparticles and Hph when the polymer grafts are absent.

However, as hypothesized, a strong interaction was observed between the SiO$_2$NP-PCL-PEG copolymer grafted particles and Hph. This was manifested as a significant increase in the total scattering of the copolymer-grafted nanoparticle solutions upon the addition of Hph. The observed signal was clearly much higher than the sum of the individual scattering profiles of Hph and SiO$_2$NP-PCL-PEG (Fig. 6a). Elsewhere the incorporation of hydrophobic molecules has been reported to enhance the association between unimolecular micelles thereby resulting in the formation of larger structures;[34] however, in the case of SiO$_2$NP-PCL-PEG, no changes in the D_h and

exhibit a distinct advantage over traditional self-assembled micelles, particularly in open systems, such as large bodies of water where dilution is inevitable.

The "nanoparticle micelle" behavior of the copolymer grafted nanoparticles was confirmed by DLS and UV experiments. The evolution of the light scattering at 90° (LS90^o) and D_h with concentration, c, for SiO$_2$NP-PCL-PEG was compared with solutions of Corexit, a commercially used dispersant in water (Fig. 7). LS based methods are routinely employed in the determination of cmcs, due to the fact that conformational changes at the onset of the micellization influence the scattering profile of the molecules, leading to an abrupt change in the scattered intensity as the transition from unimers to micelles occurs. As seen in Fig. 7a, in the case of the SiO$_2$NP-PCL-PEG nanoparticles, there is no sign of a cmc detected as there is no change in D_h or in the slope of LS *vs*. c.

These results confirm the amphiphilic nanoparticles exhibited inherent stability to dilution down to concentrations as low as 2×10^{-6} g cm^{-3}. In addition, narrow MSD data (two representative concentration points shown in insets of Fig. 7a) indicate that no significant aggregation occurs upon dilution. In contrast, Corexit structures disaggregate when diluted, with an inherent cmc indicated by the change in LS slope in Fig. 7b. In this case, the presence of both unaggregated and associated/aggregated particles in the Corexit solutions leads to bimodal distributions and affects the light scattering based D_h values (Fig. 7b insets). At lower concentrations, the higher degree of instability results in inhomogeneous aggregates. The instability of the system and inaccuracy of the D_h measurements is demonstrated by the increasing error (error bars shown in red) at high dilution.

The ability of SiO$_2$NP-PCL-PEGs to act as nanoparticle micelles has also been evaluated against Corexit through a set of dye encapsulation studies. Using pyrene as an UV-active model hydrocarbon, the dispersing capacities of these two systems were compared by measuring UV absorption for saturated solutions of pyrene with respect to SiO$_2$NP-PCL-PEG and Corexit concentration,

respectively. As shown in Fig. 8 (UV absorbance at 335 nm, measured at t = 0), more pyrene can be dispersed in solution at higher concentrations of SiO$_2$NP-PCL-PEG or Corexit, evidenced by the increases in the absorbance values. The experimental data indicate two noteworthy trends. First, the SiO$_2$NP-PCL-PEGs do exhibit nanoparticle micelle behavior as confirmed by a linear dependence between pyrene encapsulation and nanoparticle concentration, even at extremely low concentrations. In the case of Corexit, the UV absorbance vs. c for has been found to follow two sigmoidal profiles, which when analyzed using Sigmoidal-Boltzmann equation, are in agreement with other studies on surfactants and mixtures of surfactants, indicate the presence of two or more cmcs.[41,42] Secondly, although Corexit shows competitive encapsulation capacity at the initial time points, the instability of these self-assembled structures leads to reduced encapsulation capacity when monitored with respect to increasing time (Fig. 8, upper left). The SiO$_2$NP-PCL-PEGs, on the other hand, show no change in their encapsulation capacity over the 7 days studied (Fig. 8, upper right) confirming the temporal stability expected of nanoparticle micelles; a unique advantage over traditional small molecule dispersants.

Fig. 7 Light scattering (LS90°) and D_h (with error bars, representing % of value) *vs*. c for (a) SiO$_2$NP-PCL-PEG and (b) Corexit dispersed in water; in the inset, MSD data for selected concentration data points. These data confirm the stable, nanoparticle micelle behavior of the amphiphilic nanoparticles at low concentration and the inherent instability of Corexit to dilution (note c for SiO$_2$NP-PCL-PEG in 10^{-5} g/cm^3, and for Corexit 10^{-4} g/cm^3).
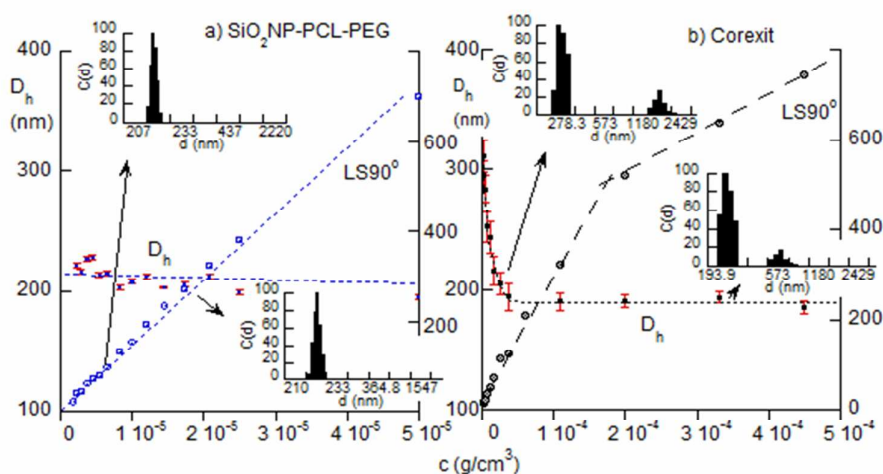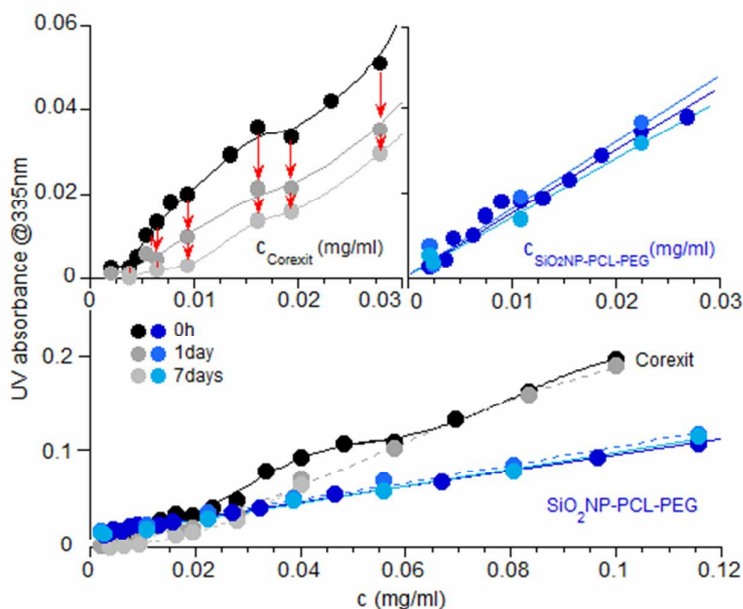
Fig. 8 The SiO$_2$NP-PCL-PEG encapsulation of pyrene (dark/light blue) measured at different times exhibits an unchanging trend of encapsulation capacity with increasing time, while the Corexit exhibits a marked decrease in encapsulation capacity (black/gray) with increasing time.

The effect of PCL length on the efficiency in encapsulating hydrophobic molecules. The modularity of each major structural parameter permits rapid tuning of their physical properties and encapsulation capacity. For dispersant applications, a longer PCL block was targeted, as this might be expected to increase the hydrophobic pocket size, and therefore increase the oil loading capacity of each nanoparticle. The PCL length could be tailored either by controlling the ROP duration or by reinitiating successive polymerizations with additional monomer. UV experiments were then used to assess the SiO$_2$NP-PCL-PEG's efficiency in encapsulating hydrophobic molecules as a function of PCL chain length, and compared to traditional dispersants, such as Corexit. Both pyrene and Hph were explored as hydrophobic guest molecules.

Using a quantitative dye release study, the encapsulation capacities of different grafted nanoparticles were compared in UV experiments designed to quantify the entrapment kinetics and the loading capacity of the nanoparticles. The nanoparticles were dispersed in an aqueous solution containing Hph in concentrations above its water-solubility. This mixture was then introduced in a dialysis membrane with a small molecular weight cut-off that would only allow Hph to traverse the membrane but not the nanoparticles. Finally, the dye+nanoparticle-loaded membrane was immersed in a reservoir containing pure water under mechanical stirring. The Automatic Continuous Mixing (ACM) technique was used to monitor the release of the excess, non-encapsulated Hph through the membrane pores by continuously measuring UV absorbance of the aqueous reservoir solution outside the dialysis membrane (see inset to Fig. 9). In this case, ACM utilized an HPLC pump to circulate sample liquid from aqueous reservoir through a detector train to acquire real-time data. By circulating the solution in the aqueous reservoir continuously through the UV detector, a continuum of data points was collected which corresponded to the amount of dye released from the nanoparticles and offered information on stability and dynamics of the solutions monitored relative to changes in experimental conditions.

The examples shown in Fig. 9 depict the release of free Hph (computed from UV data at 220 nm) through the membrane pores during the dialysis experiments of grafted nanoparticles (1:10 ratio by weight of nanoparticle to Hph) after being exposed to nanoparticles with different PCL thicknesses: single layer of PCL (about 15% PCL by weight) referred to as "SiO$_2$NP-PCL-PEG" and double layer of PCL (about 30% PCL by weight) referred to as "SiO$_2$NP-2xPCL-PEG". Data was also acquired from SiO$_2$NP-GPS (which did not include polymer grafts but did have a hydroxylated surface) to be used as control data. The observed results show a significant amount of Hph released through the dialysis membrane when studying ungrafted SiO$_2$NP-GPS, which exhibited almost complete release of the dye (~ 95 %) in 1 h.

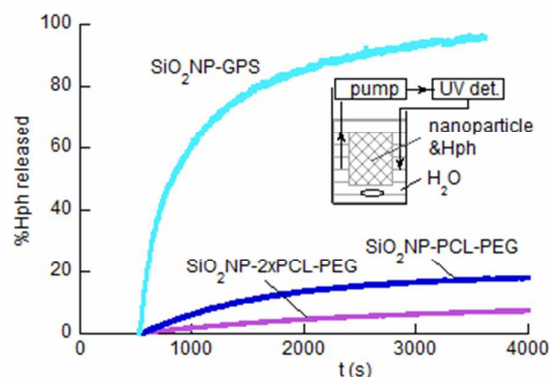Fig. 9 UV monitoring of free Hph released through dialysis membrane from SiO$_2$NP-PCL-PEG *vs*. ungrafted SiO$_2$NPs confirms a significant capacity for encapsulation in the case of the amphiphilic grafted nanoparticles. Data from amphiphilic nanoparticles with a doubled PCL thickness (SiO$_2$NP-2xPCL-PEG) exhibit an increase in encapsulation, confirming the role of the PCL layer.

However, a substantially reduced release (confirming encapsulation of Hph by the grafted nanoparticles) was observed for both the single PCL layer nanoparticles and the double layer nanoparticles,

the SiO$_2$NP-PCL-PEG retaining 81 % of the hydrophobic dye (19 % release) after 1 h, and the double layer SiO$_2$NP-2xPCL-PEG retaining 91 % of the dye (only 9 % released) after 1 h. The control studies with SiO$_2$NPs without the polymer grafts demonstrate negligible sequestration of the Hph by the nanoparticle core alone, confirming the importance of the block-copolymer architecture for hydrocarbon encapsulation. Using the same experimental conditions (1:10 (w/w) dispersant to Hph), it was found that while SiO$_2$NP-PCL-PEG loading capacity is somewhat lower than that exhibited by Corexit (which retaining more than 95 % of the dye versus 81% for the nanoparticles) doubling of the PCL layer imparts upon the SiO$_2$NP-2xPCL-PEG nanoparticles a comparable loading capacity (91%) with respect to preliminary studies of Corexit (95%).

Discrete UV experiments investigating pyrene sequestration also exhibited a boost in encapsulation upon doubling the PCL layer, supporting the conclusion from the Hph trapping studies using continuous ACM measurements. Excess pyrene was added to the aqueous nanoparticle solutions (0.1 mg mL^{-1}) with different PCL block lengths and, after filtering off the undissolved dye, UV spectra were acquired. When a comparison was made between SiO$_2$NP-PCL-PEG and Corexit, UV data (at 335 nm) indicated that Corexit could load about twice the amount of pyrene than the single layer SiO$_2$NP-PCL-PEG and 1.6 times as much as the double layer SiO$_2$NP-2xPCL-PEG (Figure S17). However, while the Corexit did initially exhibit an slightly increased loading capacity when compared to either amphiphilic nanoparticle over the first hour, the nanoparticle dispersants' ability to retain their payload capacity even after 7 days based on light scattering experiments makes them a more attractive dispersant for applications where long term stability is critical.

Conclusions

A rapid and modular approach to synthesizing amphiphilic copolymer-grafted nanoparticles was employed to produce "nanoparticle micelles" with key advantages over traditional small molecule dispersants particularly in dilute open-water environments. These amphiphilic nanoparticles were prepared by grafting a hydrophobic layer of PCL from SiO$_2$NPs, and then coupling an outer hydrophilic layer PEG onto the nanoparticle periphery. The resultant amphiphilic nanoparticles exhibited stable dispersions in aqueous medium even at extremely low concentrations, confirming the hypothesis that such structures should behave similarly to unimolecular micelles. Furthermore, detailed light-scattering studies verified the effective encapsulation of small hydrophobic molecules by the grafted nanoparticles, and confirmed the hypothesis that these nanoparticles would exhibit a stable-long term encapsulation unlike traditional small-molecule dispersants. As a comparison, the standard dispersant, Corexit, was also evaluated. Although Corexit exhibited a slightly better initial encapsulation capacity, it also exhibited poor long-term stability, as demonstrated by its continuously decreasing encapsulation capacity with respect to time. These results confirm the most promising feature of the amphiphilic nanoparticle based dispersants: their long term stability when applied in large volumes of water. Although additional optimization will be required before providing a commercially feasible alternative to Corexit or other small molecule dispersant systems, the inherent modularity of the SiO$_2$NP-PCL-PEG design should expedite the development of competitive nanoparticle-based dispersant systems.

Acknowledgements

Notes and reference

[1] M. A. Cowell, T. C. G. Kibbey, J. B. Zimmerman and K. F. Hayes, *Environ. Sci. Technol*. 2000, **34**, 1583.

[2] A. Shioi, R. Nagaoka and Y. Sugiura, *J. Chem. Eng. Jpn*. 2000, **33**, 679.

[3] G. R. Newkome, C. N. Moorefield, G. R. Baker, M. J. Saunders and S. H. Grossman, Monomolecular Micelles. *Angew. Chem. Int. Ed. Eng.* 1991, **30**, 1178.

[4] C. J. Hawker, K. L. Wooley and J. M. J. Frechet, *J. Chem. Soc., Perkin Trans. 1* 1993, **12**, 1287.

[5] D. A. Tomalia, V. Berry, M. Hall and D. M. Hedstrand, *Macromolecules* 1987, **20**, 1164.

[6] M. T. Morgan, M. A. Carnahan, C. E. Immoos, A. A. Ribeiro, S. Finkelstein, S. J. Lee, and M. W. Grinstaff, *J. Am. Chem. Soc.* 2003, **125**, 15485.

[7] Y. H. Kim and O. W. Webster, *J. Am. Chem. Soc.* 1990, **112**, 4592.

[8] A. Sunder, M. Kramer, R. Hanselmann, R. Mulhaupt and H. Frey, *Angew. Chem. Int. Ed.* 1999, **38**, 3552.

[9] F. Wang, T. K. Bronich, A. V. Kabanov, R. D. Rauh and J. Roovers, *Bioconj. Chem.* 2005, **16**, 397.

[10] A. Heise, J. L. Hedrick, C. W. Frank and R. D. Miller, *J. Am Chem. Soc.* 1999, **121**, 8647.

[11] G. L. Cheng, A. Boker, M. F. Zhang, G. Krausch and A. H. E. Müller, *Macromolecules* 2001, **34**, 6883.

[12] V. Heroguez, Y. Gnanou, and M. Fontanille, *Macromolecules* 1997, **30**, 4791.

[13] A. Pavia-Sanders, S. Zhang, J. A. Flores, J. E. Sanders, J. E. Raymond and K. L. Wooley, *ACS Nano* 2013, **7**, 7552-7561.

[14] Z. Luo, X. Cai, R. Y. Hong, L. S. Wang and W. G. Feng, *Chem. Eng. J.* 2012, **187**, 357.

[15] M. Motornov, R. Sheparovych, R. Lupitskyy, E. MacWilliams and S. Minko, *J. Colloid Interface Sci.* 2007, **310**, 481.

[16] X. Mei, D. Chen, N. Li, Q. Xu, J. Ge, H. Li and J. Lu, *Microporous Mesoporous Mat.* 2012, **152**, 16.

[17] W. Ji, N. Li, D. Chen, X. Qi, W. Sha, Y. Jiao, Q. Xu and J. Lu, *J. Mat. Chem. B* 2013, **1**, 5942.

[18] M. Marini, M. Toselli, S. Borsacchi, G. Mollica, M. Geppi and F. Pilati, *J. Polym. Sci. Pol. Chem.* 2008, **46**, 1699.

[19] A. B. Lowe, B. S. Sumerlin, M. S. Donovan and C. L. McCormick, *J. Am. Chem. Soc.* 2002, **124**, 11562.

[20] R. B. Pernites, E. L. Foster, M. J. L. Felipe, M. Robinson and R. C. Advincula, *Adv. Mater*. 2011, **23**, 1287.

[21] R. Jordan, K. Graf, H. Riegler and K. K. Unger, *Chem. Commun.* 1996, **9**, 1025.

[22] D. Mecerreyes, R. Jérôme and P. Dubois, *Adv. Polym. Sci.* 1999, **147**, 1.

[23] J. Heuschen, R. Jérôme and P. Teyssie, *Macromolecules* 1981, **14**, 242.

[24] E. Duquesne, D. Rutot, P. Degee and P. Dubois, *Macromol. Symp.* 2001, **175**, 33.

[25] M. J. Mondrinos, R. Dembzynski, L. Lu, V. K. Byrapogu, D. Wootton, M. P. I. Lelkes and J. Zhou, *Biomaterials* 2006, **27**, 4399.

[26] V. V. Seregin and J. L. Coffer, *Biomaterials* 2006, **27**, 4745-4754.

27 M. Joubert, C. Delaite, E. Bourgeat-Lami and P. Dumas, *New J. Chem.* 2005, **29**, 1601.

28 J. Pyun, S. Jia, T. Kowalewski, G. D. Patterson and K. Matyjaszewski, *Macromolecules* 2003, **36**, 5094.

29 Y. P. Wang, X. W. Pie, X. Y. He and K. Yuan, *Eur. Polym. J.* 2005, **41**, 1326.

30 H. Mori, D. C. Seng, M. F. Zhang and A. H. E. Muller, *Langmuir* 2002, **18**, 3682.

31 E. Forgacs and T. Cserhati, CRC Press LLC, Boca Raton, 1997, Vol. 3, p125.

32 S. Li, X. Jiao and, H. Yang, *Langmuir* 2013, **29**, 1228.

33 D. P. Norwood, E. Minatti and W. F. Reed, *Macromolecules* 1998, **31**, 2957-2965.

34 R. K. Kainthan, C. Mugabe, H. M. Burt and D. E. Brooks, *Biomacromolecules* 2008, **9**, 886.

35 G. Riess, *Prog. Polym. Sci.* 2003, **28**, 1107.

36 J. F. Gohy, *Adv. Polym. Sci.* 2005, **190**, 65.

37 E. B. Zhulina and O. V. Borisov, *Macromolecules* 2012, **45**, 4429.

38 H. B. Liu, A. Jiang, J. A. Guo and K. E. Uhrich, *J. Polym. Sci. Pol. Chem.* 1999, **37**, 703.

39 O. G. Schramm, G. M. Pavlov, H. P. van Erp, M. A. R. Meier, R. Hoogenboom and U. S. Schubert, *Macromolecules* 2009, **42**, 1808.

40 W. Cao and L Zhu, *Macromolecules* 2011, **44**, 1500.

41 J. Aguiar, P. Carpana, J. A. Molina-Boliver and, C. C. Ruiz *J. Colloid Interface Sci.* 2003, **258**, 116.

42 G. B. Ray, I. Chakraborty and S. P. Moulik, *J. Colloid Interface Sci.* 2006, **294**, 248.

Polymer Chemistry Accepted Manuscript

FOR TABLE OF CONTENTS ONLY

Modular amphiphilic copolymer-grafted nanoparticles: "nanoparticle micelle" behavior enhances utility as dispersants

Muhammad Ejaz, Alina M. Alb, Karolina A. Kosakowska, and Scott M. Grayson*
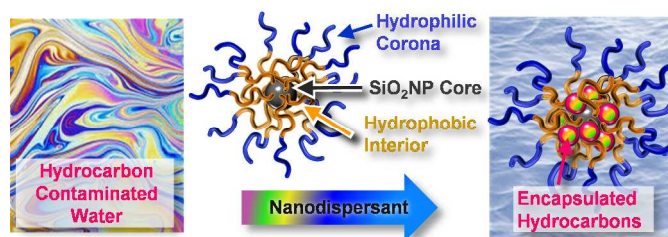
Nanoparticles with amphiphilic polymer grafts exhibit increased stability as dispersants relative to traditional small molecule amphiphiles